J Solid State Electrochem (2005) 9: 646–652
DOI 10.1007/s10008-004-0639-1

ORIGINAL PAPER

M. Miranda-Hernández · M. E. Rincón

Carbon paste electrodes: correlation between the electrochemical hydrogen storage capacity and the physicochemical properties of carbon blacks

Received: 9 September 2004 / Revised: 12 October 2004 / Accepted: 25 November 2004 / Published online: 8 February 2005

Abstract The difficulties in the use of carbon paste electrodes to quantify the electrochemical adsorption of hydrogen in nanocarbon materials are described. Chronoamperometry studies using a Ferro/Ferri redox couple were performed to obtain the electrochemical active area of paste electrodes prepared by dispersion of differing samples of carbon blacks (CB) within silicon oil. This electrochemical active area was combined with the BET-surface area of the carbon blacks, to obtain the mass of superficial carbon involved in the electrochemical processes. To assure equal conditions for comparison, the electronic conductivity of the paste was equivalent in all the samples. From our results it appears that cyclic voltammetry, combined with carbon paste electrodes and nitrogen adsorption isotherms, provides a simple and less expensive route for the qualitative evaluation of the electrochemical hydrogen uptake of novel carbon materials. Still, for quantitative measurements, some issues remain unsolved in highly structured carbons, where the lack of penetration of the bulky Ferro/Ferri redox couple in the micropores of the CB and the occurrence of solid-state diffusion cause the underestimation of the mass involved in hydrogen adsorption.

Keywords Carbon paste electrodes · Electrochemical hydrogen storage · Nitrogen isotherms

Introduction

Carbon based composites continue to be one of the most studied materials, due to the cost, availability and the broad spectra of physicochemical properties they can convey [1]. Most recently, the need of hydrogen storage in the development and broad use of fuel cells has renewed the interest in the material's design based on nanocarbon compounds [2–17]. The apparent high pressure requirement (10–12 MPa) and the need of alkaline metals in carbon materials to obtain 4–10 wt.% hydrogen adsorption from the gas phase [16], make the electrochemical hydrogen storage an attractive alternative [7–15, 17]. Furthermore, voltammetry has proved to be a fast method for the evaluation of the hydrogen storage ability of carbon materials [9–12, 18,19]. In particular, important differences in the electrochemical adsorption and evolution of hydrogen on modified carbon black (CB) paste electrodes were distinguished and explained in terms of the different physicochemical properties of the CB particles [18, 19].

In this work, we attempt the quantitative evaluation, reported in wt%, of the electrochemical hydrogen uptake of carbon paste electrodes prepared by dispersion of CBs within silicon oil (S). The use of oils is a common practice in carbon paste electrodes, where it is intended for the characterization and fast regeneration of the electrode surface. Still, the mass of carbon in the paste does not represent the electrochemical active mass of the electrode, due to the hydrophobic nature of silicon oil that avoids penetration of aqueous electrolytes. Therefore, we combined the BET-surface area of various experimental samples of CBs with the determination of the electrochemical active surface and the electrochemical response of paste electrodes in alkaline media. The results obtained provide evidence of different storage mechanisms in the carbon paste electrodes, leading to the conclusion that the properties of the carbon surface are critical for the validity of the methodology proposed. For highly structured CBs with large DBPA index, the diffusion of hydrogen and/or its solubility in silicon oil causes an underestimation of the mass of carbon involved in the electrochemical hydrogen uptake.

M. Miranda-Hernández · M. E. Rincón (✉)
Centro de Investigación en Energía-UNAM,
Apartado Postal 34, Temixco, 62580, México
E-mail: merg@cie.unam.mx
Tel.: +52-555-6229748
Fax: +52-777-3250018

Experimental

Carbon blacks powders with different surface area were supplied by Columbian Chemical Company. The morphology of these materials was obtained by high-resolution electron microscopy using a Philips TECHNAI F20 scanning transmission electron microscope. The BET-surface area was obtained from Nitrogen isotherms recorded at 77.3 °K in a TriStar (Micromeritics) apparatus. Table 1 presents some of the characteristics of the CBs tested, which were labeled: CDX, CDX-T, and 40220. CDX and 40220 are turbostratic CBs with 246 $m^2\ g^{-1}$ and 595 $m^2\ g^{-1}$ surface area, respectively. The graphitized CB CDX-T (80 $m^2\ g^{-1}$) corresponds to CDX subjected to thermal treatments at 2,200 °C in inert atmosphere.

Electrochemical measurements in 6 M KOH aqueous electrolyte were carried out with a Basic Autolab W/PGSTAT30&FRA system. A conventional tri-electrode cell, consisting of a working carbon paste electrode, graphite counter-electrode, and a Hg/HgO/1 M KOH reference electrode (+0.2 V vs. NHE), was used in the cyclic voltametry and Chronoamperometry experiments. Both reference and counter electrodes were kept in separate compartments. The paste electrodes were prepared by mixing 0.112 g of CB with silicon oil in the weight ratio of CB:S 35:65. The paste was supported in a 0.4 mm thickness Teflon ring (0.96 cm^2) with stainless steel as the back contact. All the experiments were conducted under stationary conditions and nitrogen flow to avoid oxygen diffusion and the acidification of the bulk solution due to dissolved CO_2. For quantitative measurements, the bulk resistivity and the electrochemical active area of the various paste electrodes were determined with the Ferro/Ferri cyanide reaction. Additionally, to assure similar interfacial conditions and good reproducibility, each experiment was run in a renewal surface.

Results and discussion

Microstructure and BET-surface area

Examples of the structures of CBs particles used in this study are presented in the electron micrographs of Fig. 1. Figure 1a shows an electron micrograph of the CDX (246 $m^2\ g^{-1}$) CB evidencing some ordering in the planes near the periphery of the particle. The incipient ordering is enhanced by heat treatment at 2,200 °C, as shown in Fig. 1b, where the occurrence of discrete faceting is also observed. The 60% reduction in the surface area of CDX-T is consistent with its hermetic structure. For CB 40220 (595 $m^2\ g^{-1}$), the electron micrograph evidences a superior density of growth centers and the concentric growth of carbon layer planes around them. These aggregates of carbon-anion like structures have been used as precursors for the growth of multiwalled carbon nanotubes due to the large number of pentagon and heptagon defects in the graphene lattice, which is the key for solid state diffusion [20]. These defects can also be thought as reactive hydrogen adsorption/diffusion sites and might explain the nonlinear correlation between BET surface areas and the electrochemical hydrogen uptake discussed below.

Nitrogen-adsorption isotherms of the three samples of CB are shown in Fig. 2. They resemble very closely the N_2 adsorption isotherms reported for as grown and oxidized single-walled carbon nanotubes [21]. In these CBs samples, minimum differences are observed in the values of adsorption energy (ΔG) summarized in Table 1, although important differences are evident in the volume adsorbed. The small difference in ΔG most likely reflects differences in porous distribution, since CBs are usually inert substrates for nitrogen gas adsorption. For all the carbon specimens, the adsorbed volume increased abruptly at small relative pressure due to the presence of the large amounts of micropores. Since the nitrogen gas molecule is sized 0.35 nm in diameter, the adsorbed volume measured by nitrogen gas adsorption method includes even micropores smaller than several nanometers.

Electrochemical measurements for the evaluation of the electrochemical active area of carbon paste electrodes

Bulk resistivity

The bulk resistivity of the paste electrodes was monitored against the Ferro/Ferri cyanide reaction. Here, cyclic voltammetry studies were performed on an electrolyte solution containing 0.01 M Ferro/Ferri cyanide and 1 M KCl. Figure 3 shows the typical electrochemical response of this redox couple obtained with the various carbon paste electrodes. The quasi-reversible behavior of the curves indicates good electronic conductivity in all the electrodes. The difference in peak intensities reflects the difference in electrochemical active area discussed below, while the dispersion on peak potentials (below 80 mV) is in agreement with the differences in surface functionality of the CBs.

Table 1 Physico-chemical properties of the various carbon blacks

Sample	Particle size (nm)	BET-area ($m^2\ g^{-1}$)	$\Delta G_{adsorption}$ (kJ/mol)	DBPA (ml/100 g)	Annealing T (°C)
CDX	16	246	−16.1	170	–
CDX-T	28	80	−16.9	165	2,200
40220	8	595	−17.3	225	–

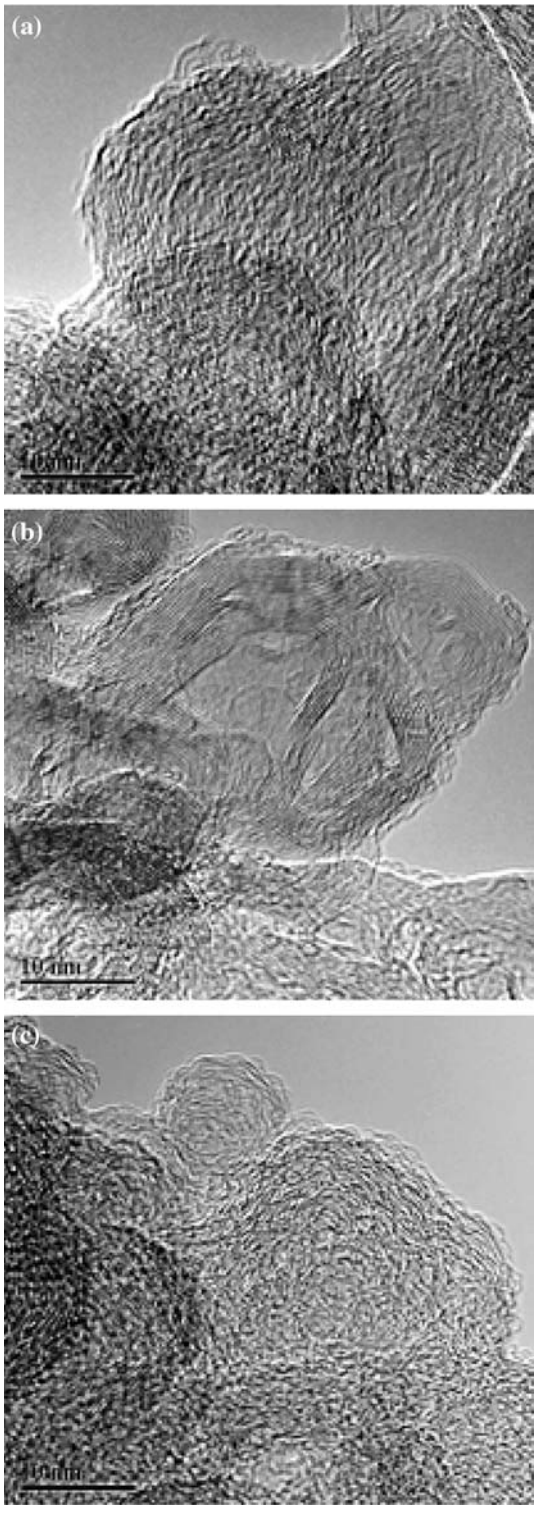

Fig. 1 TEM micrographs of the powders studied: **a** turbostratic CB (CDX) **b** graphitized CB (CDX-T) **c** high structure carbon black (CB-40220)

Electrochemical active area

The electrochemical active areas were evaluated by Chronoamperometry studies in the potential interval of 0.150–0.450 V versus SCE. According to the Cottrell

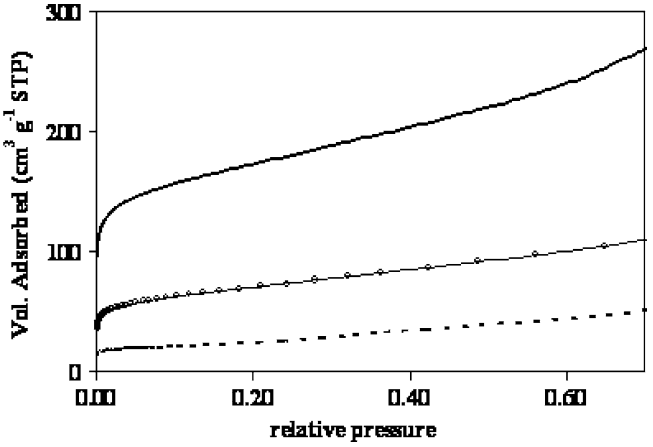

Fig. 2 Nitrogen adsorption isotherms obtained at 77 °K for CBs 40220 (*solid line*), CDX (*line-circle*), and CDX-T (*dashed line*). See Table 1 for the physicochemical description of these samples

equation (1), the slope of the linear region of the current (I) versus time $(t)^{-1/2}$ plot provides the electrochemical active area (A) if other parameters are known.

$$I = \frac{nFD^{1/2}CoA}{\pi^{1/2}t^{1/2}} \tag{1}$$

Here, n is the number of electrons exchange, F, the Faraday constant taken as 96,500 C/mol, D, the diffusion coefficient of the Ferricyanide specie (7.6×10^{-6} cm^2 s^{-1}), and C_o, the initial concentration of the electroactive specie (10^{-2} molcm^{-3}). Figure 4 shows I versus $t^{-1/2}$ plots for the various paste electrodes. Each curve goes through zero and represents the behavior observed at the various potential pulses, assuring the reliable determination of the electrochemical active areas given in Table 2. From these results, it is clear that a good correlation exists between the BET-surface area of the CB component and the electrochemical active area of the paste electrode. The BET-surface area of the

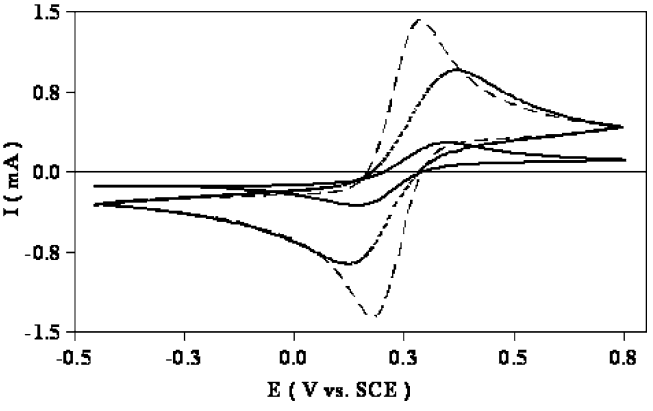

Fig. 3 The quasi-reversible behavior of the 0.01 M Ferro/Ferri cyanide redox pair in aqueous 1 M KCl, assures the good electronic conductivity of the CB-40220 (*dash line*), CDX (*short dash line*), and CDX-T (*solid line*) carbon-paste electrodes

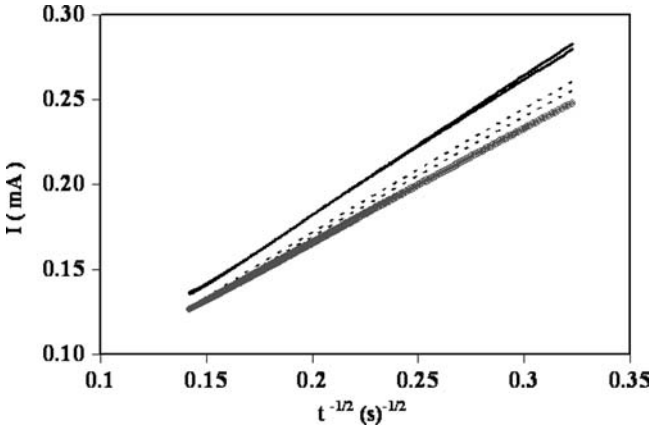

Fig. 4 Chronoamperograms of carbon-paste electrodes shown as I versus $t^{-/2}$ plots: 40220 (*solid line*), CDX (*circles*), and CDX-T (*dashed line*). CDX (*circles*), CDX-T. Data obtained by the potential step technique in a 0.01 M Ferro/Ferri cyanide/1 M KCl solution

electrode, calculated from the mass of CB used in the paste, is compared with the electrochemical value. This comparison is shown in Table 2 and plotted in Fig. 5. In the figure we have also added another sample of CB with only 5 m^2 g^{-1} BET-surface area. Clearly, the significant difference in the values plotted indicates that only few micrograms of carbon are involved in the electrochemical reaction. It corresponds to the first superficial layers of the paste. In a first approximation, this mass ($C_{superficial}$) can be calculated from the electrochemical active area of the paste electrode divided by the BET-surface area of the CB component. The major drawback in this approximation is the fact that the ferrous/ferric ions are so large in size that they cannot penetrate into the pores with sizes of nanometers [22]. Therefore, for CBs with a large fraction of micropores, the electrochemically active area determined in 0.01 M ferrous/ferric cyanide solution will be much lower in value than the one determined by the nitrogen gas adsorption

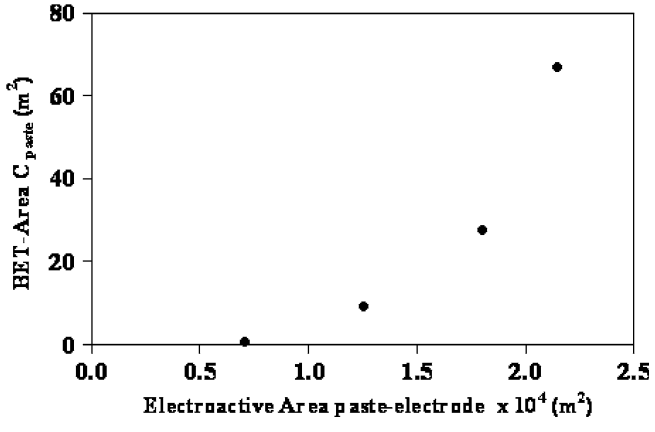

Fig. 5 Correlation between the measured electrochemical active area and the estimated BET-surface area of various CB-paste electrodes

Table 2 Determination of the amount of carbon black (CB) electrochemically active in different paste electrodes

Sample	BET area -C^a_{paste} (m^2)	Electroactive area × 10^4 (m^2)	$C^b_{surface}$ (μg)
CDX	28	1.81	0.73
CDX-T	9	1.26	1.57
40220	67	2.15	0.36

[a]From: (mass of CB) × (BET-area CB)
[b]From: (electroactive area)/(BET-area CB)

method. For these CBs, the methodology proposed will underestimate the mass of CBs involved in the electrochemical process.

Electrochemical hydrogen uptake mechanisms and quantification

Mechanisms

The electrochemical hydrogen adsorption on carbon materials relies on the dissociation of water at the working electrode ($C + H_2O + e- \rightarrow C–H_{ads} + OH^-$). The hydrogen storage capacity of the electrode is obtained through the inverse reaction (oxidation), which measures the amount of adsorbed atomic hydrogen that intercalates in the carbon material plus the amount that recombines into molecular hydrogen and diffuses into the electrode. The amount of cathodic charge that cannot be recovered in the anodic process is what escapes as hydrogen gas bubbles. These different stages depend not only on the electrochemically active sites, but also on the porosity of carbon, and can be followed by Cyclic Voltammetry studies in alkaline media. We performed these experiments in the potential range of 0.6 V to −1.5 V versus Hg/HgO/1 M KOH, initiating at rest potential (V_r) and going in the negative direction at a scan rate of 50 mV/s. At this rate, the adsorption equilibrium is difficult to establish in porous materials due to the small effective diffusion coefficient, giving a sluggish response upon potential inversion. Still, inferior scan rates compromise the signal/noise ratio, causing problems in the detection of small faradic currents, which are then dominated by the electrostatic charging of the double layer.

Figures 6, 7, and 8 report the voltammograms of the various carbon paste electrodes during the first two cycles. The electrochemical response of the electrode based on CDX (Fig. 6) shows slow and irreversible processes plus the activation of the surface with cycling. That is, the reduction peaks C_1 and C_2 observed during the first cycle (we use 'C' for cathodic events, and 'A' for anodic events; with the sub-index indicating the order of appearance) are better resolved and shift to less negative potentials during the second cycle. More important, they are accompanied by an intense cathodic peak (C_3) preceding hydrogen evolution. Moreover, magnification of the anodic processes around −0.6 V versus Hg/HgO/1 M KOH occurs during the second cycle, while the electrode response (i.e. recording of positive current) becomes faster upon inversion of the potential at −1.5 V

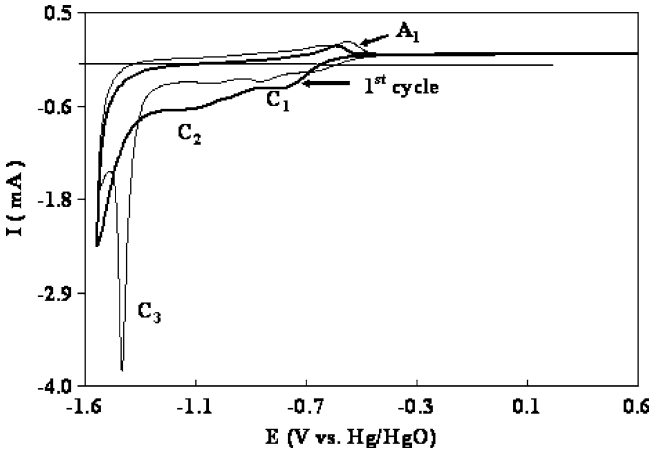

Fig. 6 Cyclic voltammograms showing the first cycles for the electrochemical hydrogen uptake of CDX paste electrodes immersed in aqueous 6 M KOH. Scans initiating from rest potential in the negative direction at 50 mV/s. Electrode geometric area = 0.96 cm^2

versus Hg/HgO/1 M KOH. It is also notorious the lack of current in the potential interval of −0.4 V to 0.6 V that rules out electrochemical oxidation as the origin of C_3. On the other hand, the decrease of C_1 and C_2 with the number of cycles suggests the depletion of the electroactive species in the carbon paste. The correlation of C_1/C_2 with the anodic peak (A_1) has been validated in other works and corresponds to the redox processes of the carbon surface functional groups [7, 11]. For the redox processes associated to hydrogen storage, it is evident that only the cathodic peak C_3 is well defined, while the anodic peak related to hydrogen desorption is not observed at 50 mV/s.

The effect of annealing on the electrochemical response of CDX-T is shown in Fig. 7. Note the change in current scale evidencing the inferior electrochemical responses of the processes C_1 and C_2 on graphitized CB. They move to more negative potentials and are less intense, in agreement with the reduction on surface

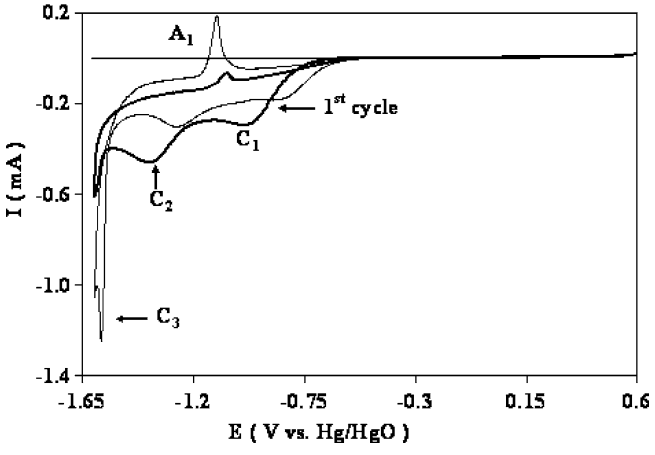

Fig. 7 Cyclic voltammograms recorded at 50 mV/s for the electrochemical hydrogen uptake of CDX-T paste electrodes immersed in aqueous 6 M KOH. Scan initiating from rest potential in the negative direction. Electrode geometric area = 0.96 cm^2

area and surface functionality (i.e., carbon–oxygen complexes) after thermal treatment. Here again, activation of the carbon surface shifts C_1/C_2 to more positive potentials and causes the appearance of C_3 during the second cycle. For this electrode, the effect of graphitization is more evident in the anodic signals. Unlike the CDX electrode, the electrode based on CDX-T shows the presence of a narrow peak associated with the electrochemical desorption of hydrogen (i.e., $H_{ads} - e^- \rightarrow H^+$). It seems that the hermetic structure of this carbon helps toward a fast electrochemical response, with little interference of diffusive processes. Some factors to consider are: (a) the electroactive surface is mainly at the basal planes of graphene layers, and (b) the loss of surface functionality contributes to a narrow distribution of reactive sites, and therefore, to a sharp oxidation peak. The clear increment in the size of the basal plane after graphitization (Fig. 1) and the fact that the conductive and capacitive properties of edge and basal planes are different from each other [23, 24], led to the conclusion that for thermally treated carbons, the properties of the basal planes determine the hydrogen uptake mechanism.

For CB 40220, Fig. 8 shows a different electrochemical response when compared to CDX or CDX-T electrodes. Intense capacitive currents mask the reduction processes associated to native carbon–oxygen complexes (see inset). The well-defined hydrogen adsorption peak (C_3) is not observed in this material. Moreover, the anodic current in the potential interval of −1.4 V to −0.7 V versus Hg/HgO/1 M KOH appears as a limiting current, suggesting the substantial accumulation of hydrogen in the paste. This electrode has an oxidation process at ~0.5 V versus Hg/HgO/1 M KOH, which can be associated with the adsorption of OH^- or the oxidation of the carbon surface [7, 18, 19]. In general, the electrochemical response of this material agrees with its large surface area and the abundance of surface defects, and the absence of the peak associated with the adsorption of atomic hydrogen suggests the fast recombination of these atoms into molecular hydrogen.

The data presented support different hydrogen storage mechanisms in the carbon-paste electrodes. A dominant role of basal planes in the graphitized CDX-T CB, confines the adsorption/desorption of atomic hydrogen at the outer surface ($H_{ads} - e^- \rightarrow H^+$; $C_{basal\ planes}$). In the electrode based on turbostratic CDX CB, contribution from the CB inner surface is important, and hydrogen desorption is affected by surface diffusion processes ($H_{ads} - e^- \rightarrow H^+$; C_{bulk}). For CB 40220, the storage of molecular hydrogen inside the paste is evident, and the anodic response is associated to the oxidation of molecular hydrogen ($H_{2\ ads} - 2e^- \rightarrow 2H^+$; C_{paste}).

Quantification of the electrochemical hydrogen uptake

The electrochemical hydrogen storage of the various carbon paste electrodes is reported in Table 3 and

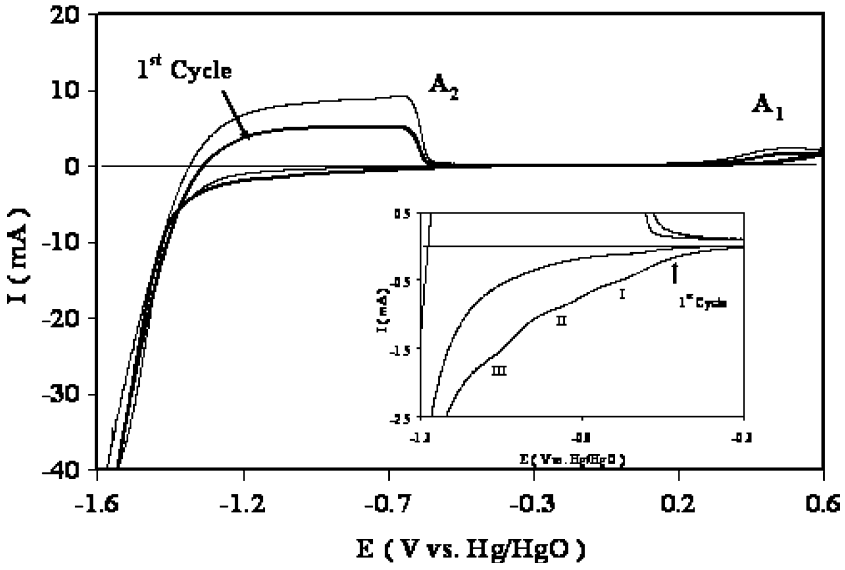

Fig. 8 Cyclic voltammograms showing the first cycles for the electrochemical hydrogen uptake of CB-40220 paste electrodes immersed in aqueous 6 M KOH. Scans initiating from rest potential in the negative direction at 50 mV/s. Electrode geometric area = 0.96 cm^2. The inset shows the magnification of the cathodic peaks observed in the first scan

plotted in Fig. 9 as a function of polarization time. Polarization experiments were performed at −1.525 V versus Hg/HgO. This potential is slightly superior to the value of E_{peak} (C_3) in CDX and CDX-T, but corresponds to incipient hydrogen evolution in CB 40220. The extrapolation to zero polarization time is intended to minimize the contribution of molecular hydrogen (i.e. to obtain the amount of charge corresponding to adsorbed atomic hydrogen). Table 3 reports the amount of charge applied (or recovered) converted to wt.% hydrogen adsorption by means of the mass of superficial carbon reported in Table 2. As explained before, the presence of micropores led to the underestimation of the mass of carbon on the electrode surface; thus the values of adsorption capacity per unit mass reported in Table 3 must be considered the upper limits for the real adsorption capacity. For CDX and CDX-T the numbers reported in Table 3 are reasonable and several orders of magnitude higher than the values obtained using the mass of CB in the paste. For the paste based on CB-40220, even the calculated hydrogen capacity at zero polarization time is several orders of magnitude above the expected adsorption capacity of carbon materials [13]. To date, the highest value of 1.5–2% was found for activated carbon samples subjected to nitric acid treatment, which renders 3.5 meq/g total surface functionality (mostly carbon–oxygen complexes). Therefore, it is clear that in this electrode, the methodology proposed has another source of error in addition to the abundance of micropores: the abundance of structural defects assisting solid state diffusion, which is consistent with the high structure of CB-40220 (obtained from DBPA values).

Conclusion

In this work, we use carbon paste electrodes to quantify the electrochemical hydrogen uptake of various CBs, using the specific surface area obtained from N_2-isotherms and the electrochemical active surface obtained from Chronoamperometry studies. Cyclic voltammetry

Table 3 Storage of Hydrogen in carbon blacks-paste electrodes as a function of polarization time at −1.52 V versus Hg/HgO. Electrodes immersed in 6 M KOH

Sample	Pol. time (s)	Q^a_{pol} (mC)	Q^b_{des} (mC)	H_{des} (μg)	H_{des}/C_{surf} %	H_{des}/C_{paste} %
CDX	0	–	0.02	1.7E-04	0.02	1.5E-07
	90	11.43	0.02	1.7E-04	0.02	1.5E-07
	300	20.07	0.26	2.7E-03	0.37	2.4E-06
	1,200	86.70	4.28	4.5E-02	6.10	4.0E-05
CDX-T	0	–	0.01	9.9E-05	0.01	8.8E-08
	90	0.8	0.01	9.9E-05	0.01	8.8E-08
	300	1.6	0.28	2.9E-03	0.18	2.6E-06
	1,200	1.2	0.40	4.2E-03	0.26	3.7E-06
40220	0	–	2.5	2.6E-02	7	2.3E-07
	90	48.7	4.0	4.2E-02	12	3.7E-05
	300	111	14	1.5E-01	41	1.3E-04
	1,200	312	41	4.3E-01	119	3.8E-04

Q_{pol}: charge accumulated during the initial polarization period
Q_{des}: charge integrated from the anodic potential scan at 10 mV/s

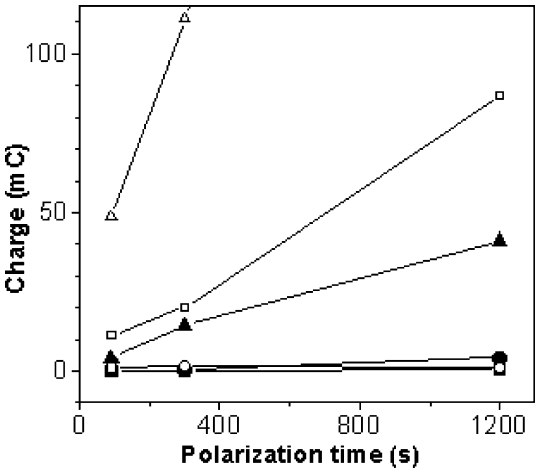

Fig. 9 Electrochemical hydrogen uptake as a function of polarization time for carbon paste electrodes based on CDX (*filled circle*, *open circle*), CDX-T (*filled square*,*open square*) and CB- 40420 (*filled triangle*, *open triangle*). Polarization experiments were performed at −1.525 V versus Hg/HgO. Open symbols correspond to the charge accumulated during the initial polarization, and solid symbols to the charge integrated during the anodic potential sweep at 10 mV/s

studies suggest various mechanisms and active sites for electrochemical hydrogen storage, which seem to correlate not only with the surface area of CBs, but also with their kind of structural defects. The good correlation validates the use of carbon paste electrodes as a powerful tool for the evaluation of novel carbon materials with low microporosity. Still, for quantitative measurements, some issues remain unsolved due to the superior diffusion of hydrogen in carbon paste electrodes based on highly structured CBs. In these materials, the hydrophobic nature of silicon oil is not enough to confine the electrochemical hydrogen uptake to the electrode surface. The direct evaluation of the diffusion coefficient and the electrochemical active area for the hydrogen reaction in paste electrodes are currently under progress in Electrochemical Impedance Spectroscopy studies.

Acknowledgments The authors are grateful to M.E. Trujillo-Camacho and R. Moran for technical assistance, to DGAPA-UNAM and CONACYT-MEXICO for financial support.

References

1. Kinoshita K (2003) Carbon, electrochemical and physicochemical properties. Wiley, New York
2. Ye Y, Ahn CC, Witham C, Fultz B, Liu J, Rinzler AG, Colbert D, Smith KA, Smalley RE (1999) Appl Phys Lett 74:2307
3. Dillon AC, Bekkedahl TA, Jones KM, Heben MJ (1999) Fullerenes 3:716
4. Wu HB, Chen P, Lin J, Tan KL (2000) Int J Hydrogen Energy 25:261
5. Yang RT (2000) Carbon 38:623
6. Yin YF, Mays T, McEnaney B (2000) Langmuir 103:10521
7. Barisci JN, Wallace GG, Baughman RH (2000) J Electroanal Chem 488:92
8. Rajalakshmi N, Dhathathreyan KS, Govindaraj A, Satishkumar BC (2000) Electrochim Acta 45:4511
9. Lee SM, Park KS, Choi YC, Park YS, Bok JM, Bae DJ, Nahm KS, Choi YG, Yu SC, Kim N, Frauenheim T, Lee YH (2000) Synthetic Metals 113:209
10. Qin X, Gao XP, Liu H, Yuan HT, Yan DY, Gong WL, Song DY (2000) Electrochem Solid State Lett 3:532
11. Jurewicz K, Frackowiak E, Béguin F (2001) Electrochem Solid State Lett 4:A27
12. Gao XP, Lan Y, Pan GL, Wu F, Qu JQ, Song DY, Shen PW (2001) Electrochem Solid State Lett 4:A173
13. Frackowiak E, Béguin F (2002) Carbon 40:1775
14. Züttel A, Sudan P, Mauron P, Kiyobayashi T, Emmenegger C, Schlapbach L (2002) Int J Hydrogen Energy 27:203
15. Youn HS, Ryu H, Cho TH, Choi WK (2002) Int J Hydrogen Energy 27:937
16. Darkrim FL, Malbrunot P, Tartaglia GP (2002) Int J Hydrogen Energy 27:193
17. Yan X, Gao X, Li Y, Liu Z, Wu F, Shen Y, Son D (2003) Chem Phys Lett 372:336
18. Miranda-Hernández M, Ayala JA, Rincón ME (2003) J Solid State Electrochem 7:264
19. Miranda-Hernández M, Ayala JA, Rincón ME (2003) J Solid State Electrochem 7:264
20. Buchholz DB, Doherty SP, Chang RPH (2003) Carbon 41:1625
21. Fujiwara A, Ishii K, Suematsu H, Kataura H, Maniwa Y, Suzuki S, Achiba Y (2001) Chem Phys Lett 336:205
22. Strømme M, Niklasson GA, Granqvist CG (1995) Phys Rev B 52:14192
23. Groszek AJ (1987) Carbon 25:717
24. Qu D (2002) J Power Sources 109:403